# Integrating topographic knowledge into deep learning for the void-filling of digital elevation models

Sijin Li[1,2,3,4], Guanghui Hu[1,2,3], Xinghua Cheng[5], Liyang Xiong[1,2,3]*, Guoan Tang[1,2,3], Josef Strobl[2,4]

1. School of Geography, Nanjing Normal University, Nanjing, 210023, China;

2. Key Laboratory of Virtual Geographic Environment (Nanjing Normal University), Ministry of Education, Nanjing, 210023, China;

3. Jiangsu Center for Collaborative Innovation in Geographical Information Resource Development and Application, Nanjing, 210023, China;

4. Department of Geoinformatics – Z_GIS, University of Salzburg, Salzburg 5020, Austria;

5. Department of Land Surveying and Geo-Informatics, The Hong Kong Polytechnic University, KLN, Hong Kong, China.

***Corresponding author:** Liyang Xiong, **E-mail**: xiongliyang@njnu.edu.cn

**Statement of Author Contribution:** Sijin Li and Liyang Xiong provided the initial idea; Sijin Li, Guanghui Hu and Liyang Xiong designed the methodology and performed the experiment; Guanghui Hu and Xinghua Cheng contributed to the data analysis and the result assessment; Sijin Li, Xinghua Cheng and Guoan Tang contributed to writting the paper; Liyang Xiong and Guoan Tang provided the funding; Xinghua Cheng, Guoan Tang and Josef Strobl reviewed the manuscript.

**Abstract:** Digital elevation models (DEMs) are some of the most important data for providing terrain information and supporting environmental analyses. However, the applications of DEMs are significantly limited by data voids that commonly exist in regions with rugged terrain and remove topographic features carried by DEMs. We propose a novel deep learning-based strategy called a topographic knowledge-constrained conditional generative adversarial network (TKCGAN) to fill data voids in DEMs. Shuttle Radar Topography Mission (SRTM) data with the spatial resolution of 3 and 1 arc-seconds are used in the experiments to demonstrate the applicability of the TKCGAN. The qualitative topographic knowledge of valleys and ridges is transformed to new loss functions that can be applied in deep learning-based algorithms and constrain the training process. The results show that the TKCGAN outperforms other common methods to fill voids in DEMs and can improve the elevation and slope accuracy of the reconstructed results. The performance of TKCGAN is stable in test areas and significantly reduce the error in the regions with medium and high slope. Furthermore, the analysis of profile maps reflect that TKCGAN achieve better performance from the perspective of visual inspection and quantitative comparison. In addition, the proposed strategy can be applied to DEMs with different resolutions. This work is an endeavour to transform perceptive topographic knowledge into computer-processable rules, and this approach can benefit future research related to terrain reconstruction and modelling.

**Keyword:** DEM reconstruction; topographic constraints; terrain features; conditional generative adversarial network

## 1. Introduction

Land surfaces consist of multiple landforms and contain various topographic characteristics (Evans, 2012; Xiong et al., 2021; Zhao et al., 2019). These different types of terrain are shaped by various forces and carry a large amount of information that can support the related Earth science researches. Digital elevation models (DEMs), as one practical way to digitally present the Earth's surface, have been widely applied in geographical studies, such as land use change analysis, disaster monitoring, geographical feature detection and ecosystem modelling (Chou et al., 2010; Ozouville et al. 2008, Sesnie et al., 2008; Wei et al., 2021; Xiong et al., 2014). In the past years, a range of DEM datasets have been freely launched with the improvement of Earth observation techniques. However, due to the limitations of the existing observation techniques, data voids exist in several DEM datasets, including Shuttle Radar Topographic Mission (SRTM) and Advanced Spaceborne Thermal Emission and Reflection Radiometer (ASTER) Global Digital Elevation Model version 2 (GDEMV2) (Ling et al., 2007; Robinson et al., 2014). One reason for the generation of data voids is the influence of rough surfaces on the signals emitted by sensors, especially those carried by spacecraft (Dong et al., 2020; Hall et al., 2005). For example, in mountain areas, complex terrains with various elevation and slope differences interfere with signals and cause a large number of voids in ridge and valley areas (Boulton and Stokes, 2018; Dong et al., 2020; Hall et al., 2005). Such data voids significantly result in the loss of topographic information and hence reduce the validity of related research (Boulton and Stokes, 2018; Robinson et al., 2014).

To address issues of filling voids and missing DEM data, various methods have been developed. One possible method for DEM reconstruction is manual treatment including the data

67 filling based on field surveys and other alternative observations. However, currently, it is not
68 recommended due to its high cost of time and labour (Dong et al., 2020; Li et al., 2020b).

69 The combination of different DEMs provides a possible way to produce non-void DEM
70 through the integration of auxiliary DEM from other sources (Karkee et al., 2008; Ling et al.,
71 2007; Milan et al. 2011). For example, ASTER GDEMV2 and the GMTED2010 elevation
72 model are used to filling the voids in SRTM and help to produce complete SRTM data. However,
73 some difficulties prevent the improvement of this technique. Usually, previous DEMs that are
74 available for the void-filling have unsatisfactory quality and coarse resolution compared with
75 novel dataset, and hardly meet the accuracy requirement of the current DEMs. The integration
76 process would result in the loss of terrain information and nonuniform quality in the integrated
77 DEM (Ling et al., 2007; Milan et al., 2011). Moreover, auxiliary DEMs are not always available
78 in void areas, which also limits the application of this kind of technique.

79 Several interpolation methods, such as Kriging, spline and inverse distance weighting
80 (IDW), have been widely adopted in geographical research as a feasible technique for void
81 filling especially in specific cases with good performance (Dong et al., 2020; Reuter et al.,
82 2007). Nevertheless, due to the lack of observations causing ‘holes’, the results of interpolation
83 methods are significantly influenced by the terrain characteristics around the void regions,
84 resulting in discontinuous and obvious boundaries at joints (Dong et al. 2020; Grohman et al.,
85 2006). Thus, a range of interpolation-based methods that integrate topographic cues around
86 void areas have been proposed to generate suitable terrain representations over incomplete
87 regions (Arun 2013; Heritage et al., 2009; Ling et al., 2007; Reuter et al., 2007). However,
88 interpolation methods is hard to fill incomplete DEMs in areas with complex terrain because

89 they are implemented based on local characteristics, which lack the consideration of the global
90 information contained in non-void regions and would result in the reconstructed data having
91 inconsistent topographic characteristics compared with those of the neighbouring areas without
92 voids. (Dong et al., 2019; Dong et al., 2020).

93 Following the development of machine learning, deep learning-based techniques have
94 received extensive attention given their powerful learning abilities (Dong et al., 2020; Li and
95 Hsu, 2020; LeCun et al., 2015). They are capable of learning not only local characteristics but
96 also global information and contextual features (Li et al., 2020a; Li and Hsu, 2020; Yuan et al.,
97 2020). Previous studies have proven that deep learning-based models achieve good
98 performance in geographical research (Li et al., 2017, 2020b; Lu et al. 2017). A generative
99 adversarial network (GAN) (Goodfellow et al., 2014) is a type of convolutional neural network
100 (CNN) and it includes an adversarial structure and therefore sidesteps the difficulty of
101 approximating many intractable probabilistic computations (Goodfellow et al., 2014, Zhu et al.,
102 2020). One GAN variant, called the conditional generative adversarial network (CGAN)
103 (Gauthier, 2014; Mirza and Osindero, 2014), has been widely used in terrain modelling (Qiu et
104 al., 2019; Zhu et al., 2020). In the field of DEM reconstruction, the learning and inference
105 abilities of the CGAN can support the extraction of latent topographic information and the
106 terrain reconstruction in non-data areas with consistent topographic characteristics (Dong et al.,
107 2020).

108 DEMs are the digital representation of the real surface, and carry a large amount of terrain
109 information (Xiong et al., 2014, 2021). Missing data usually occur in areas with complex terrain
110 characteristics that disturb the detection of sensors (Dong et al., 2019, Farr et al., 2007).

Reconstruction algorithms without topographic constraints that can influence the training process usually achieve unsatisfactory results in these rugged areas (Dong et al., 2020; Zhu et al., 2020). Additionally, smoothing effects, which can be viewed as reductions in and losses of terrain information, also have the relation with the lack of consideration of the inherent topographic characteristics (Dong et al., 2020; Reuter et al., 2007). Previous studies have attempted to integrate topographic cues into void-filling algorithms as constraints and provide models to restore DEMs with additional terrain information (Qiu et al., 2019; Zhu et al., 2020). These topographic cues include valley lines (Ling et al., 2007), hill shading (Dong et al., 2019) and textures (Qiu et al., 2019). However, even features containing terrain knowledge have been considered in void-filling methods in different ways, such approaches still need to determine (i) which type of terrain knowledge can efficiently improve the quality of the restored DEM and (ii) how to integrate these valuable topographic cues into advanced techniques to generate a complete DEM with much terrain information.

This study proposes a topographic knowledge-constrained CGAN method to improve the validity of reconstructed DEM and to recover key terrain features. The topographic knowledge related to terrain feature lines is summarized and transferred in a practical way to constrain the training processes of deep learning models.

## 2. Materials and methods

### 2.1 Topographic knowledge as constraints for DEM reconstruction

Topographic knowledge represents a combination of the perceptive description about the topographic characteristics across different environments. For example, a valley is

characterized by a thalweg, and a mountain is characterized by a summit (Guilbert and Moulin, 2017; Xiong et al., 2021). It is necessary to emphasize topographic knowledge during DEM reconstruction because the general constraints at the pixel level may be ineffective when we hope to fix voids of DEMs with reliable terrains. For example, in Figure 1, even though Figures 1(b) and (c) have the same root mean square errors (RMSEs), the terrains expressed by these two figures should not be viewed as the same due to the different slope and ridge direction. This indicates that it is possible to reconstruct DEMs with good accuracy at the pixel level but with unexpected terrain. An incorrect expression of terrain can result in inaccurate predictions and the loss of terrain characteristics, thereby damaging the applications of reconstructed DEMs. Therefore, in this study, we hope to construct a strategy that not only emphasize the basic elevation accuracy but also integrate qualitative topographic knowledge into a deep learning-based algorithm and discuss the potential influence on the subsequent geographic analysis.

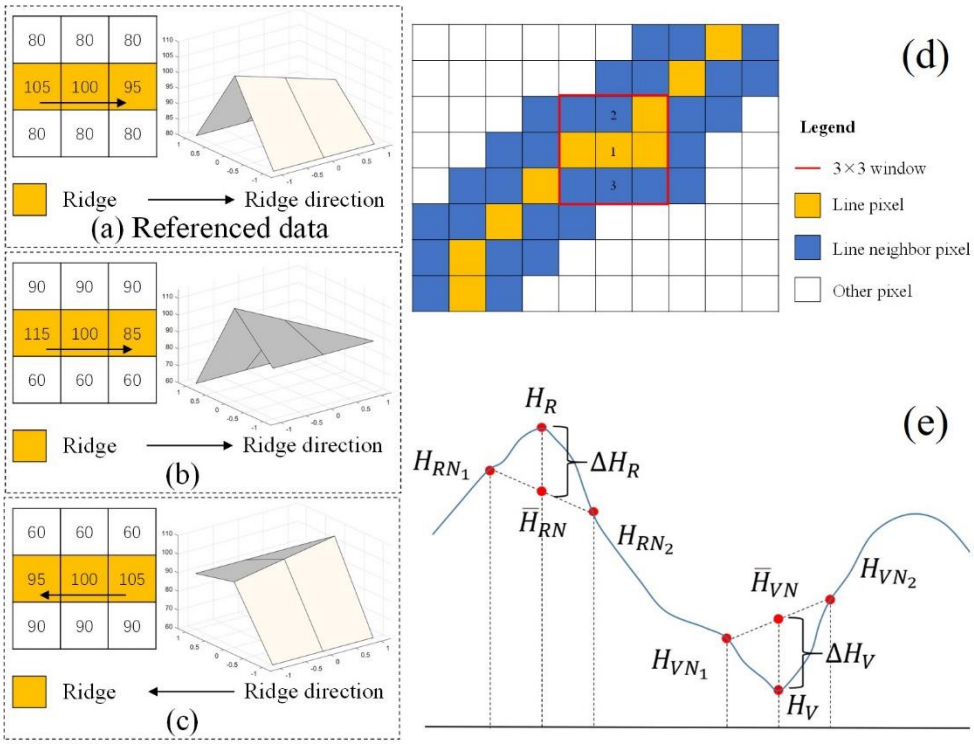


**Figure 1**. Representations of surfaces with different topographic characteristics. (a) is the

referenced terrain data, while (b) and (c) are assumed reconstructed results generated by different methods. (d) is the representations of line and LN pixels. (e) reflect the geometries in ridge and valley areas.

A large area of voids in DEMs can be observed in the regions around valleys and ridges especially in mountainous areas. On the one hand, rugged surfaces and variable weather increase the difficulty of producing DEMs with correct topographic characteristics (Qiu et al., 2019). On the other hand, the side-looking characteristics possessed by some sensors can also result in a large number of voids in these areas because large areas of terrain interfere with detection signals (Dong et al., 2020). These voids erase valleys and ridges that carry the basic terrain structure and significant topographic information. Therefore, we introduce ridge and valley lines as additional features in deep learning-based algorithms and build quantitative rules that are transferred from qualitative concepts to guide the learning processes of these algorithms. These quantitative and computer-processable rules can be combined with deep learning-based algorithms and guide the process of terrain generation.

Before the introduction of the topographic knowledge used in this study, we hope to define a new term: 'line neighbour' (LN). LNs are defined as the regions adjacent to terrain lines. For example, as shown in Figure 1(d), line pixels represent the pixels on terrain lines (in this study, they represent valleys and ridges), and for each line pixel, LN pixels are denoted as pixels in a 3×3 window that have not been marked as terrain line pixels. The LNs in valleys and ridges, called ridge neighbours (RNs) and valley neighbours (VNs), respectively, are subsequently generated. Based on the definition of LN, a quantitative relation the number of LN pixels is three times the number of line pixels can be summarized as

$$3 * Lnum = LNnum \quad (1)$$

where $Lnum$ is the number of line pixels and $LNnum$ is the number of LN pixels. The relation of three time is an empirical value generated by our primary experiments. This equation is empirical and makes senses in most cases, even though $LNnum$ may fluctuate around the value representing three times of $Lnum$. In mountainous areas, the generation of ridge lines often parallels the generation of valleys, and valleys and ridges usually have similar numerical features. Therefore, equation (1) can be simultaneously applied to the study of valleys and ridges.

Based on the quantitative relation between $Lnum$ and $LNnum$, we modelled the topographic knowledge around ridges and valleys from two perspectives. The first characteristic that we hope to emphasized is the intensity of terrain relief that can be described as that the elevation of a ridge should be greater than that of its neighbouring area, and the elevation of a valley should be less than that of its neighbouring area. For example, in Figure 1(d), if the pixel marked by 1 is on the ridge, its elevation should be simultaneously greater than those of the pixels marked 2 and 3. Consequently, in a specific region with a suitable area and a similar landform type, the mean elevation of the ridge (valley) pixels should be greater (less) than that of the LN pixels; this can be represented by:

$$\overline{H}_L = \frac{\sum Lele}{Lnum} \quad (2)$$

$$\overline{H}_{LN} = \frac{\sum LNele}{LNnum} \quad (3)$$

where $\overline{H}_L$ is the mean elevation of the line pixels, and $\overline{H}_{LN}$ is the mean elevation of the LN pixels. $Lele$ and $LNele$ represent the elevations of each line pixel and LN pixel, respectively, while $Lnum$ and $LNnum$ denote the numbers of line and LN pixels, respectively. In equation

(2) and (3), $\overline{H}_R$ should be greater than $\overline{H}_{RN}$ in ridge areas and, $\overline{H}_V$ should be less than $\overline{H}_{VN}$ in valley areas. In a mountainous area, the values of $\overline{H}_L$ and $\overline{H}_{LN}$ usually show obvious differences. We also hope that the DEM data can depict such a difference. Thus, the third rule can be constructed as:

$$\Delta H = abs(\overline{H}_L - \overline{H}_{LN}) > H' \tag{4}$$

where $\Delta H$ is the absolute value of the difference between $\overline{H}_L$ and $\overline{H}_{LN}$, and $H'$ is the minimum elevation difference that we expect to be obtained from the DEM data. $H'$ should not be tiny; otherwise, the data cannot describe the characteristics of mountainous areas. This rule can reflect the elevation differences between the terrain line region and LNs. However, due to the use of absolute value, similar results would be obtained from ridge and valley regions and it will be difficult to respectively reflect the characteristics in ridge and valley regions. To discriminate between the different elevation relationships in valleys and ridges, the second characteristic is as the slope shape that related to the shape of profile and can distinguish the convex and concave profiles, and the corresponding equation is designed as:

$$For\ valleys, N_{V=}\frac{\overline{H}_{VN}}{\overline{H}_V} = \frac{\frac{\sum VNele}{VNnum}}{\frac{\sum Vele}{Vnum}} = \frac{\frac{\sum VNele}{3Vnum}}{\frac{\sum Vele}{Vnum}} = \frac{\sum VNele}{3\sum Vele} \tag{5}$$

$$For\ ridges, N_R = \frac{\overline{H}_R}{\overline{H}_{RN}} = \frac{\frac{\sum Rele}{Rnum}}{\frac{\sum RNele}{RNnum}} = \frac{\frac{\sum Rele}{Rnum}}{\frac{\sum RNele}{3Rnum}} = \frac{3\sum Rele}{\sum RNele} \tag{6}$$

$N_V$ and $N_R$ are the relief ration respectively in the valley and ridge regions. These equations can be used to magnify the differences between the ridge and valley features and avoid negative values, which would cause unexpected problems in the model training process. In most cases, the results of equations (5) and (6) are greater than 1. The greater the values of $N_R$ and $N_V$ are, the more intense the relief in the specific researched region.

## 2.2 Integrating topographic knowledge into the CGAN

### 2.2.1 Basic structure of the CGAN

The first GAN was originally designed by Goodfellow et al. (2014). A GAN includes an adversarial structure and thus sidesteps the difficulty of approximating many intractable probabilistic computations (Goodfellow et al., 2014). However, GANs usually only take random noise as input samples, which leads to ambiguity in the generated results. To provide conditions that can guide the generation process and improve the interpretability of the generated results, the CGAN is introduced as an extended GAN structure (Mirza and Osindero, 2014). The CGAN contains a similar adversarial structure to that of the basic GAN, but an advanced encoder-decoder architecture is used to guide the training process by the insertion of external conditions (Gauthier, 2014; Mirza and Osindero, 2014). It has been proven that the CGAN can support various data generation applications (Qiu et al., 2019; Zhu et al., 2020). The basic structure of the CGAN consists of two main parts: a generator *G* and a discriminator *D*. *G* is used to learn the information hidden in data and capture features from the data distribution. *D*, which plays a role similar to that of a 'referee', calculates the difference between the annotated data and the output of *G* and distinguishes between the real and synthetic images. The overall loss that influences the training of the CGAN is usually designed as the sum of the loss functions mentioned above:

$$L_{CGAN} = eL_1 + L_G + L_D \tag{7}$$

where $e$ is an empirical scaling parameter; $L_1$, $L_G$ and $L_D$ are three basic loss functions in the CGAN for guiding the training process (Mirza and Osindero, 2014). $L_1$ and $L_G$ exist in

$G$, while $L_D$ works in $D$. The training processes of $G$ and $D$ result in the minimization and maximization of $L_{CGAN}$, respectively (Dong et al., 2020). This model follows a two-player min-max adversarial game, and eventually, the optimal $G$ and $D$ are obtained as follows:

$$Optimal(G, D) = \min_{G} \min_{D} L_{CGAN} \tag{8}$$

$G$ and $D$ obtain the capability to generate realistic data and distinguish generated data from the ground truth data, respectively, through this competition. The expected result is that $G$ will be able to generate data that cannot be discriminated by $D$. Thus, the optimal model can be used to achieve the good performance that users expect.

### 2.2.2 Constraints for the CGAN based on topographic knowledge

The networks that rely only on the basic CGAN structure and loss functions usually do not perform well on DEM reconstruction tasks. As mentioned in Section 2.1, knowledge related to key terrain features should be emphasized in the DEM restoration process. To integrate linear terrain feature constraints into the neural network scheme, the general topographic knowledge mentioned in Section 2.1 is reframed as new loss functions to guide the training of the CGAN. We design five loss functions in this study: two for the generator and three for the discriminator. For the generator:

(1) According to equations (1), (2), (3) and (4), we can obtain a further understanding of $\Delta H$:

$$\begin{aligned} \Delta H &= \left|\frac{\sum Lele}{Lnum} - \frac{\sum LNele}{LNnum}\right| = \left|\frac{\sum Lele}{Lnum} - \frac{\sum LNele}{3\,Lnum}\right| \\ &= \left|\frac{\sum Lele}{Tnum \times \alpha} - \frac{\sum LNele}{3\,Tnum \times \alpha}\right| \\ &= \left|\frac{3\sum Lele - \sum LNele}{3\,TNum \times \alpha}\right| \end{aligned} \tag{9}$$

where $Tnum$ is the number of patches and $\alpha$ is the percentage of terrain line pixels in one

patch. The first loss function is described in equation (10) as follows:

$$L_H = |\ln(\Delta H^R_{output})| + |\ln(\Delta H^V_{output})| \quad (10)$$

where $\Delta H_{output}$ represents $\Delta H$, which is calculated based on the results generated according to equation (9); $R$ and $V$ represent the ridge and valley results, respectively. $\alpha$ reflects the percentage of terrain line pixels and can be regarded as a representation of topographic complexity. With increasing $\alpha$, the terrain becomes more complex, and the numerator of $\Delta H$, which reflects the elevation difference between the terrain line and LN areas, also increases due to the working principle of $L_H$.

(2) As mentioned in the previous section, equation (10) cannot completely describe the features of valleys and ridges. Therefore, a new loss function based on equations (5) and (6) with a terrain feature cue is formed as follows:

$$L_N = ln|N_R \times \beta| + ln|N_V \times \beta| \quad (11)$$

where $N_R$ and $N_V$ have been introduced in the original equation (5) and (6). $\beta$ has a similar influence to that of $\alpha$ in equation (9), and it is also set as a user-defined parameter. During the training process, $\beta$ control the intense of terrain relief and the model with high beta tends to construct high elevation difference in ridge and valley regions. The above two loss functions are applied in the GAN generator.

For the discriminator:

(1) The function of the discriminator is to calculate the difference between the target data and the output data. The pixels on valleys and ridges are significant for restoring DEMs with our method. Therefore, we define a loss function to emphasize the disagreements in ridge and valley areas and improve the elevation accuracy of the terrain lines.

$$L_E = \sum_{x \in X_R} \left| H_{output}(x) - H_{target}(x) \right| + \sum_{x \in X_V} \left| H_{output}(x) - H_{target}(x) \right| \quad (12)$$

$$L_{EN} = \sum_{x \in X_{RN}} \left| H_{output}(x) - H_{target}(x) \right| + \sum_{x \in X_{VN}} \left| H_{output}(x) - H_{target}(x) \right| \quad (13)$$

where $X_R$ and $X_V$ represent pixels located on valleys and ridges, respectively; $X_{RN}$ and $X_{VN}$ represent pixels located on ridge neighbours and valley neighbours, respectively; $H_{output}$ is the restored DEM generated by the generator; and $H_{target}$ is the complete DEM used for reference.

(2) To guarantee the elevation accuracy of pixels on the feature line and LN that are used in the calculation of other loss functions, the second loss function used in the discriminator is formulated as follows to emphasized the accuracy at the pixel-level:

$$L_S = \left| \Delta H^R_{output} - \Delta H^R_{target} \right| + \left| \Delta H^V_{output} - \Delta H^V_{target} \right| \quad (14)$$

where $\Delta H_{output}$ and $\Delta H_{target}$ represent $\Delta H$s that are calculated based on output data and target data, respectively, according to equation (9); *R* and *V* represent results for valleys and ridges, respectively.

### 2.2.3 Topographic knowledge-constrained CGAN

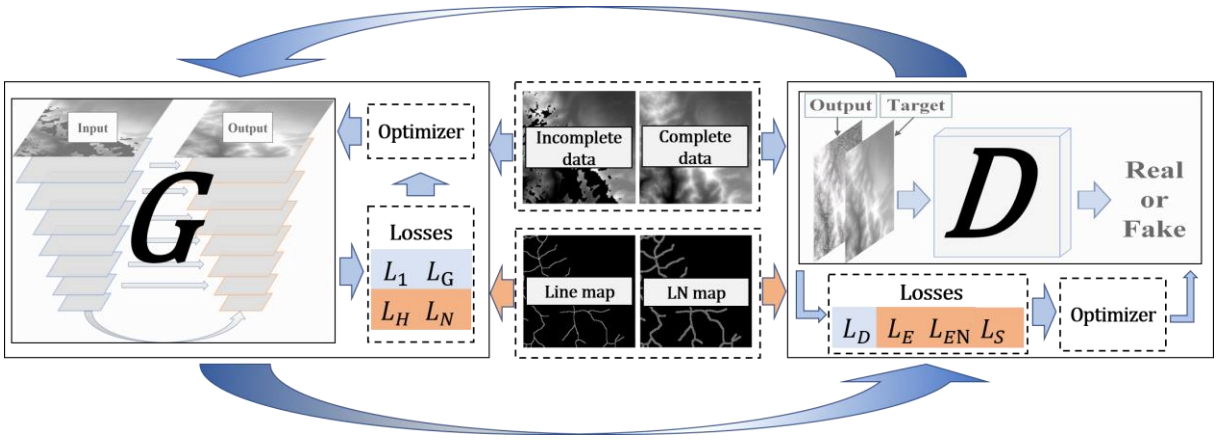


**Figure 2**. TKCGAN structure. It is formed from two basic parts, generator *G* and discriminator *D*. The traditional loss functions of CGAN are marked by blue and the new

input features and loss functions are marked by orange.

Motivated by the previous sections, we propose a new CGAN constrained by topographical knowledge, which is called the terrain knowledge-constrained CGAN (TKCGAN) as shown in Figure 2. The TKCGAN inherits the basic structure of the CGAN and consists of *G* and *D*. Incomplete and complete DEMs are used as the original inputs of the whole model, and the corresponding terrain line map and an LN map are also introduced to provide additional terrain information. The overall loss function of the TKCGAN consists of two basic functions and the three new functions mentioned in Section 2.2.2; this complete function is shown as follows:

$$L_{TKCGAN} = L_{CGAN} + \omega_H L_H + \omega_N L_N + \omega_E L_E + \omega_{EN} L_{EN} + \omega_S L_S \quad (15)$$

where $\omega_H$, $\omega_D$, $\omega_E$, $\omega_{EN}$ and $\omega_S$ represent parameters that can balance the effects of different components. Following equation (7), the optimal *G* and *D* can be obtained through the adversarial game. The Adam optimizer is employed in the TKCGAN to separately minimize G and maximize *D*. During the training process, the model learns the data distribution of the DEM under the constraints of the topographic knowledge-based loss functions. The new model is not only driven by the training data but also constrained by geometric rules, which enable the TKCGAN to encode 'potential' knowledge about terrain characteristics and generate reasonable results.

### 2.3 Evaluation method

To assess the performance of the TKCGAN, we compare the results obtained by kriging interpolation, IDW interpolation, the traditional CGAN and the TKCGAN in the same test areas. The complete data that will be mentioned in Section 2.4 is regarded as the reference

313 data in the result assessment. The comparison of different methods is performed from three
314 perspectives. (1) Visual inspection is firstly utilized to establish the plausibility of the
315 reconstructed results. (2) A composite evaluation is employed to assess the reconstructing
316 performances from the perspective of pixel level and topographic characteristics. At first, we
317 prepared the results generated by different methods and the corresponding complete data, and
318 then calculated the slope, which can be regarded as one of the most significant terrain
319 derivatives, based on these elevation data. After that, we computed the elevation and slope
320 difference between the complete data and the reconstructed data, and analysed the spatial
321 distribution of differences. Then, RMSE and mean absolute error (MAE) of elevation and
322 slope in the void areas are calculated to quantitatively evaluate the accuracy of the restored
323 results. RMSE and MAE are common indices for assessing the accuracy of results at the pixel
324 level, and can be viewed as a representation of global error (Reuter et al., 2007; Zheng et al.,
325 2016). RMSE and MAE are calculated as follows:

326 $$RMSE = \sqrt{\frac{1}{n}\sum_{i=1}^{n}(Z'_i - Z_i)^2} \quad (16)$$

327 $$MAE = \frac{1}{n}\sum_{i=1}^{n}|Z'_i - Z_i| \quad (17)$$

328 where $Z'_i$ and $Z_i$ represent the elevation value of the restored DEM and that of the reference
329 data at the position of pixel *i*, respectively, and n is the total number of pixels. In addition, we
330 also discuss the potential relation between the error and the slope. Finally, two entropy indices
331 are employed to assess the difference of topographic information. The theory of entropy is
332 used to measure the loss of information content (Shannon, 1948), and the resulting entropy
333 value can also reflect the spatial variability of the raster data. Shannon entropy (SE) and
334 configuration entropy (CE) are used in this step. SE, also called information entropy, is a

quantitative measure of the information content contained in a message or image (Shannon, 1948) and has been widely used in landscape ecology and geographical research (Gao et al., 2017). A high SE value is usually associated with terrain that has highly variable elevation (Wang et al., 2001). CE is the basic measure of entropy in thermodynamics (Geman and Geman, 1984) and has been applied in geographical studies related to DEMs (Cheng and Li, 2021a, 2021b; Gao et al., 2017). The most important advantage of CE is that it can measure the spatial configurations of terrain expressed by a DEM; these cannot be obtained by using SE. We calculate the SE and CE of each DEM and then compute the entropy difference as follows:

$$D_{SE} = SE_{reconstructed} - SE_{referenced} \quad (18)$$

$$D_{CE} = CE_{reconstructed} - CE_{referenced} \quad (19)$$

where 'referenced' and 'reconstructed' represent the entropy of the referenced DEM and the reconstructed DEM, respectively. The entropy difference can reflect the similarity between the terrain information and spatial configuration of the real surface and that of the restored surface. A negative value for the entropy difference indicates that the loss of terrain information has occurred in the generated results. A positive value for the entropy difference means that the corresponding algorithm constructs some extra information and creates characteristics that are not present in the reference data. Currently, we cannot certain if this information is redundant or if it represents the real land surface. Generally, a lower absolute value of the entropy difference represents less terrain information deviation and a higher similarity between the reference data and generated results. (3) The comparison based on profile maps is utilized to discuss the performances of different methods at specific locations. Several profiles are

selected in different study areas. Meanwhile, we also quantitatively evaluated the reconstructing performance in the voids on profiles through the comparison of MAE. The generation performances of the models with respect to key terrain features such as valleys and ridges can be obtained through the analysis of the produced profile maps.

### 2.4 Data and study area

The shuttle radar topographic mission (SRTM) DEM is one of the largest public DEM datasets in the world (Farr et al., 2007), and it has been widely used in geographical research. This DEM covers over 80% of the Earth's surface between the latitudes of 60°N and 56°S. Two main datasets of SRTM respectively called SRTM Non-Void Filled ([dataset] Shuttle Radar Topography Mission (SRTM) Non-Void Filled) and SRTM Void Filled ([dataset] Shuttle Radar Topography Mission (SRTM) Void Filled) released by United States Geological Survey are selected as the basic DEMs in this study. There are a large number of voids remaining in the SRTM Non-Void Filled data, and these data voids negatively influence the applications of the SRTM DEM. Later, the National Geospatial-Intelligence Agency filled the voids by the interpolation methods (Farr et al., 2007) and the auxiliary elevation data from the ASTER GDEMV2 and the GMTED2010 elevation model compiled by the US Geological Survey (Shuttle Radar Topography Mission, 2021), and then released the SRTM Void Filled dataset with no data voids. Therefore, these two types of SRTM DEMs are selected as the main data in this study. The spatial resolutions of the SRTM Non-Void Filled and SRTM Void Filled data are all 3 arc-seconds (approximately 90 m) for global coverage and 1 arc-second (approximately 30 m) for the United States. To assess the applicability of the proposed strategy for data with

different spatial resolutions, two study areas are selected. The first study area is located in Himalayas Mountain, while the second study area is in the Rocky Mountain. These two areas are all typical mountainous regions. Due to interference from complex terrain and environments, the quality of the SRTM data is not satisfactory, and a range of voids can be observed in the two abovementioned areas (Hirt, 2018). Additionally, sketches of ridge and valley lines can be used to describe the main relief structures in these mountainous areas. The characteristics can help us to discuss the functionality and efficiency of terrain features for filling DEM voids.

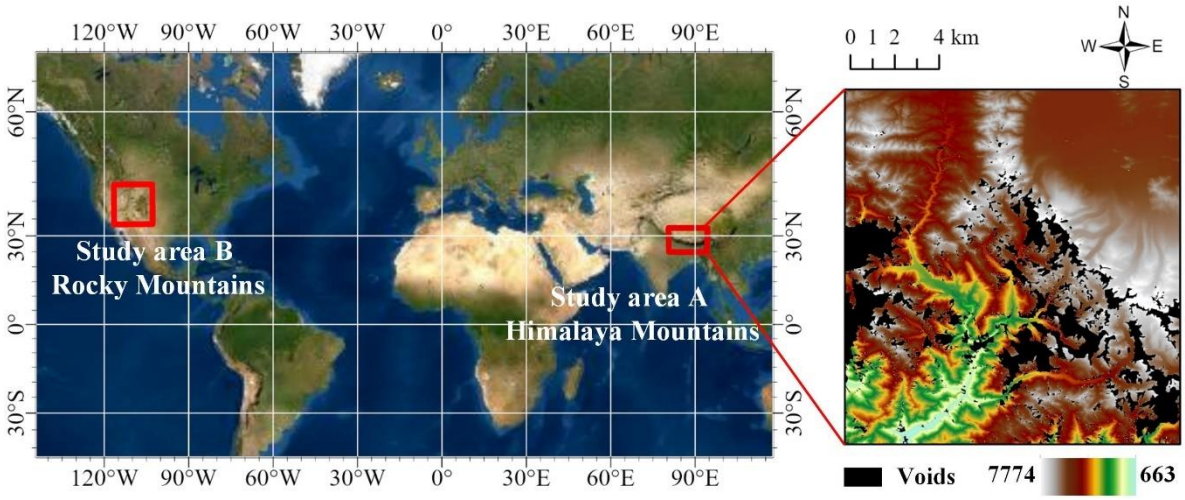


**Figure 3**. Study areas. Area A is in the Himalayas Mountain, where has many of Earth's highest peaks, including the highest, Mount Everest. Area B is in Rocky Mountain where is a major mountain range and the largest mountain system in North America. These two areas both contains various terrains and intense terrain relief which result in data voids on SRTM.

Four components of each training sample need to be prepared based on the SRTM DEM: (1) an incomplete DEM, which includes data voids; (2) a complete DEM without data voids, (3) terrain feature line maps (hereinafter referred to as line maps) and (4) LN maps. For the incomplete data, the SRTM Non-Void Filled data, which contains the original data voids, is

used for the Himalayas Mountain, while data with artificial voids produced based on the SRTM Void Filled data are regarded as the incomplete data for the Rocky Mountain. The SRTM Void Filled data is used as the complete data for two areas. Detailed information on the incomplete and complete data used in these two study areas can be found in Table 1. Then, for the line maps, we manually draw all valleys and ridges in the void areas based on remote sensing imagery. Finally, an LN map is produced based on the generated line maps. An iterative process is applied to each terrain feature line pixel and finds the pixels that have no marks, i.e., those that are not marked as terrain lines, in a 3×3 window. These selected pixels are marked as LN pixels. After the iterative process, the results are viewed as LN maps. For the TKCGAN, one training sample consists of one incomplete patch, one complete patch, one line map patch and one LN map patch. The incomplete patch is used as the input data, and the complete patch is regarded as the target of the generator *G*, which means that the output of *G* should contain elevation values and terrain characteristics similar to those of the complete data. The line and LN patch join the model when it calculates the losses based on the functions we defined before.

**Table 1**. Detailed information about the prepared dataset

| | Datatype | Data Source | Void Type | Spatial Resolution |
|---|---|---|---|---|
| **Himalayas Mountain** | Incomplete data | SRTM Non-Void Filled | Original voids | 3 arc-second |
| | Complete data | SRTM Void Filled | No voids | |
| **Rocky Mountain** | Incomplete data | SRTM Void Filled | Artificial voids | 1 arc-second |
| | Complete data | SRTM Void Filled | No voids | |

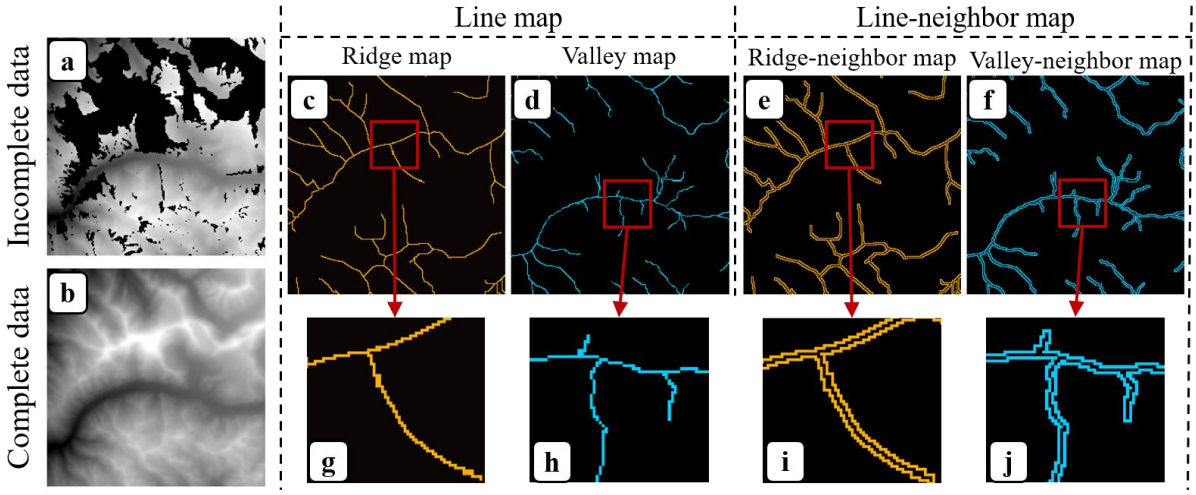


**Figure 4**. Representations of the different datasets used in the TKCGAN (samples of the Himalayas Mountain). (a) Incomplete data; (b) Complete data; (c)-(f) are respectively ridge map, valley map, ridge-neighbor map and valley-neighbor map; (g)-(j) are magnifications of red boxes respectively on figure (c)-(f).

## 3. Results

### 3.1 Filling voids in the test areas

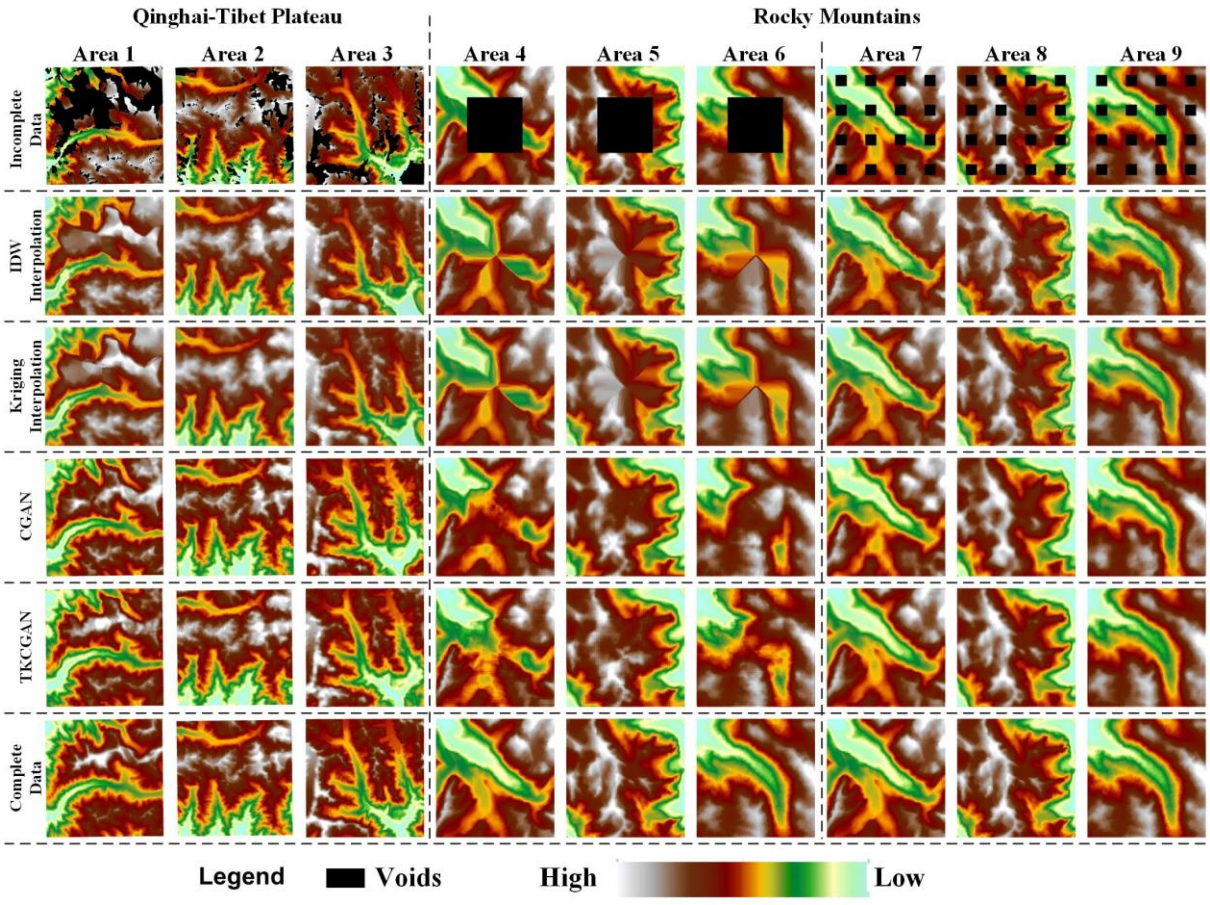


**Figure 5**. Comparison of the reconstruction results output by different methods.

Figure 5 shows the results generated by different methods. The performances of interpolation methods are not stable across the different test areas. The results of the IDW and kriging interpolation methods construct similar terrains with the referenced data in areas with small data voids such as Areas 7, 8 and 9. However, when they are used to fill large voids, the working principle of the interpolation methods leads to bad results with obvious visual effects because of the lack of enough sample points around the void areas. The CGAN and TKCGAN achieve better visual effect with reliable terrains than those of the interpolation methods,

especially in areas with large voids including Areas 1, 3, 4, 5 and 6. However, the difference between the results of the CGAN and TKCGAN is not clear from the perspective of visual inspection. In addition, the smoothing effects, which are common phenomena exhibited by algorithms based on CNNs, can still be observed in the results of the TKCGAN and CGAN. Terrain details such as small valleys are smoothed and appear blurry when reconstructed with a deep learning algorithm. The initial conclusion obtained from the visual analysis is that the CGAN and TKCGAN are better at completing the DEM reconstruction task than the IDW and kriging interpolation methods, and these networks can be applied in a variety of areas that contain voids of different sizes.

### 3.2 The assessment of elevation reconstruction: analysis of altitude error

**Table 2.** Altitude accuracy of the reconstructed result in void areas

(The best performances are highlighted in bold.)

| | RMSE (m) | | | | | MAE (m) | | | |
|---|---|---|---|---|---|---|---|---|---|
| | IDW | Kriging | CGAN | TKCGAN | | IDW | Kriging | CGAN | TKCGAN |
| **Area 1** | 103.62 | 102.59 | 104.46 | **102.91** | **Area 1** | 86.30 | 85.95 | 90.65 | **85.37** |
| **Area 2** | 93.96 | 95.28 | 101.46 | **93.08** | **Area 2** | 77.18 | 79.14 | 87.53 | **76.34** |
| **Area 3** | 106.18 | 104.09 | 108.82 | **99.38** | **Area 3** | 89.67 | 88.15 | 92.78 | **85.16** |
| **Area 4** | 84.03 | 84.52 | 112.13 | **75.24** | **Area 4** | 64.28 | 64.88 | 103.12 | **61.56** |
| **Area 5** | 87.79 | **86.12** | 96.74 | 89.95 | **Area 5** | 72.46 | **71.24** | 72.93 | 75.74 |
| **Area 6** | 86.88 | 87.19 | 90.79 | **81.04** | **Area 6** | 66.84 | 67.16 | 74.51 | **65.49** |
| **Area 7** | 40.68 | **30.44** | 46.57 | 37.13 | **Area 7** | 27.53 | **19.84** | 31.71 | 27.39 |
| **Area 8** | 50.91 | **38.52** | 42.33 | 41.16 | **Area 8** | 36.17 | **26.24** | 64.14 | 49.77 |
| **Area 9** | 27.57 | **26.84** | 49.03 | 28.74 | **Area 9** | 20.58 | **20.39** | 36.00 | 23.81 |

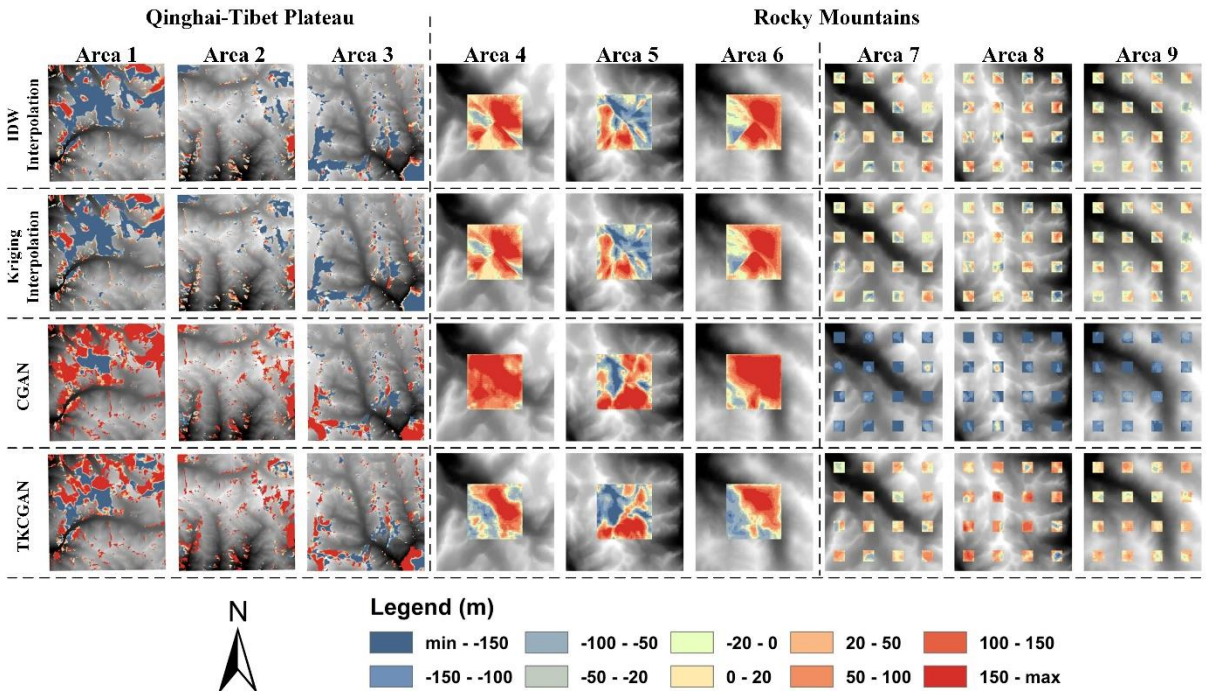


439

440 **Figure 6.** The distribution of elevation differences between reconstructed results and

441 referenced data in voids.

442 Table 2 shows the RMSE and MAE of different methods from the perspective of elevation.

443 Observations from this table indicate that TKCGAN outperforms other filling methods in areas

444 with original voids and big artificial voids, while the interpolation methods achieve better

445 performance in the rest areas with small artificial voids. This is the consistent indication with

446 what we obtained in Section 3.1. Moreover, the spatial distribution of elevation difference is

447 shown in Figure 6. The same classification scheme and colour map are applied in each area to

448 support the clear representation of the result comparison. In the Areas 1, 2 and 3 with original

449 voids, interpolation methods tend to generate significant negative errors while CGAN and

450 TKCGAN contain a large area with obvious positive errors. A significant distribution pattern

451 of elevation difference that a boundary from northwest to southeast divide the reconstructed

452 data into two regions can be observed in the results of two interpolation methods. Moreover,

453 the results of CGAN do not show significant spatial distribution of elevation difference and

contain more differences in the both original and artificial voids than that of TKCGAN. Especially in Areas 7, 8 and 9, the elevation of most pixels in the CGAN's results are much lower than that of the referenced complete data. For TKCGAN, the obvious positive elevation can be found in the valley regions in Areas 4 and 6 and this phenomenon could be caused by the a large amount of global information which contain a large amount of ridge and high elevation values.

In order to analyse the influence of terrain relief on elevation error, we present the relationship between elevation MAE and slope in Figure 7. The results of interpolation methods show obvious increasing trends with the increase of slope, while CGAN and TKCGAN generally present fluctuation with the increase of slope. The minimum elevation MAE of CGAN and TKCGAN exists in the regions with medium slope from 10 to 40 degree. In addition, the curves of TKCGAN contain considerably small differences between the maximum and minimum MAE especially in Areas 7, 8 and 9, and this phenomenon indicate the error of TKCGAN's results have an insignificant relationship with slope.

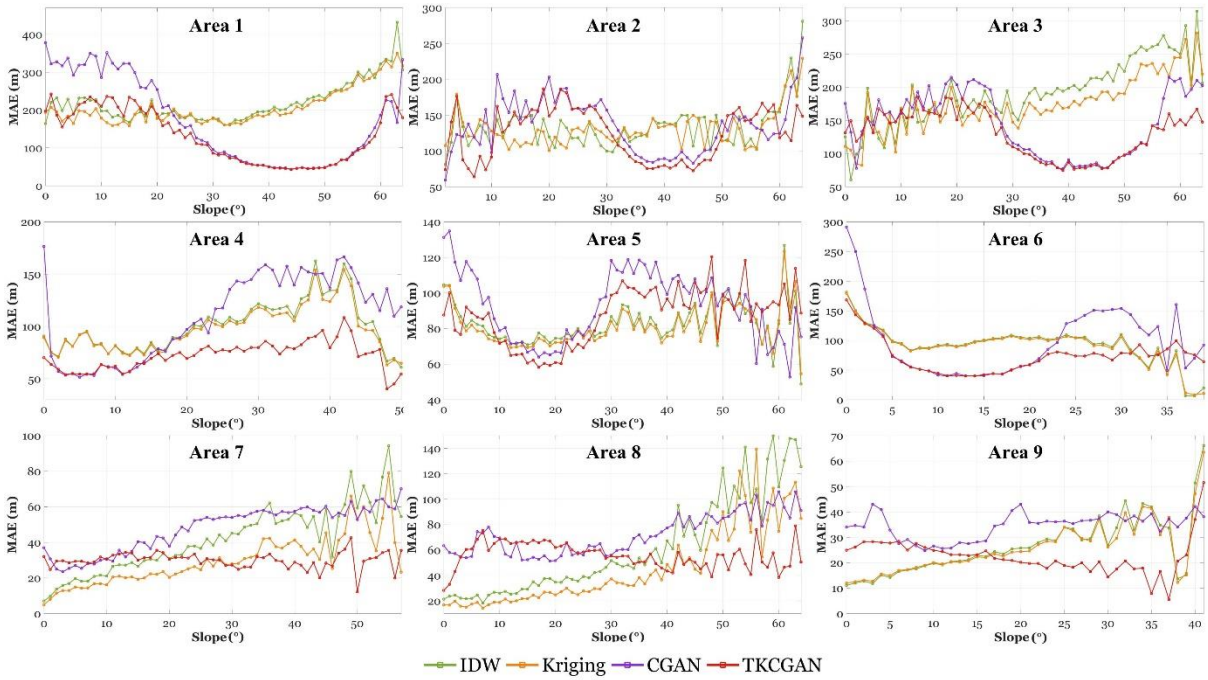


**Figure 7.** The statistical relationship between elevation MAE and surface slope of different areas.

### 3.3 The assessment of terrain reconstruction: analysis of slope and entropy difference

**Table 3** Slope accuracy of the reconstructed result in void areas

(The best performances are highlighted in bold.)

| | RMSE (°) | | | | | MAE (°) | | | |
|---|---|---|---|---|---|---|---|---|---|
| | IDW | Kriging | CGAN | TKCGAN | | IDW | Kriging | CGAN | TKCGAN |
| **Area 1** | 17.13 | 17.04 | 14.49 | **14.11** | **Area 1** | 13.26 | 13.01 | 11.36 | **11.19** |
| **Area 2** | 12.21 | **11.60** | 14.07 | 11.99 | **Area 2** | 9.83 | **9.00** | 11.24 | 9.51 |
| **Area 3** | 13.85 | 14.66 | 16.20 | **13.21** | **Area 3** | 11.02 | 11.24 | 12.92 | **10.25** |
| **Area 4** | 16.53 | 15.82 | 11.72 | **11.96** | **Area 4** | 12.59 | 11.89 | 9.33 | **9.75** |
| **Area 5** | 17.55 | 16.93 | 12.84 | **14.57** | **Area 5** | 13.41 | 13.05 | 10.41 | **10.33** |
| **Area 6** | 18.57 | 18.90 | 9.73 | **9.14** | **Area 6** | 12.51 | 13.19 | 7.88 | **7.34** |
| **Area 7** | 14.96 | 11.99 | 11.37 | **7.43** | **Area 7** | 11.03 | 8.60 | 9.39 | **6.15** |
| **Area 8** | 15.82 | 12.94 | 12.75 | **9.46** | **Area 8** | 12.34 | 9.94 | 10.42 | **7.73** |
| **Area 9** | 13.71 | 12.60 | 9.14 | **6.91** | **Area 9** | 10.34 | 9.68 | 7.65 | **5.69** |

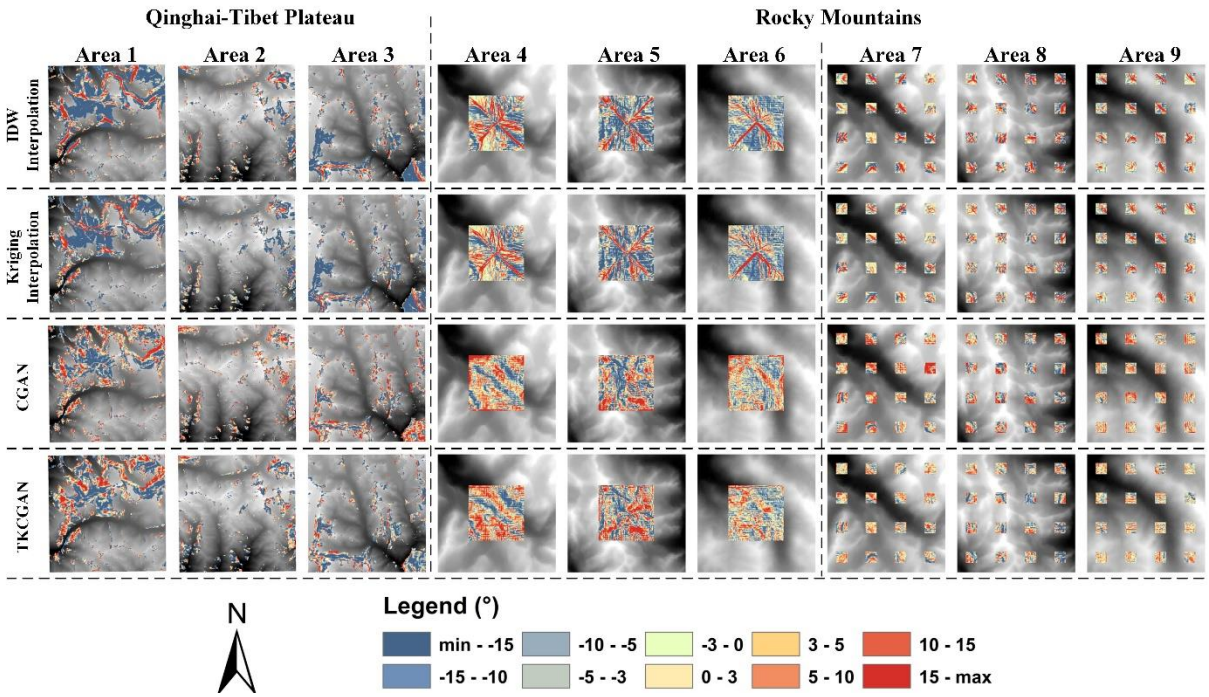


**Figure 8.** The distribution of slope difference between reconstructed results and referenced data in voids.

From the observation of Table 3, it can be noticed that TKCGAN achieve the lowest RMSE and MAE in all test areas except Area 2. It indicates that the proposed method significantly outperforms other methods from the perspective the slope analysis and is able to construct similar topographic relief with the referenced data. In addition, the spatial distribution of slope difference is shown in Figure 8. In the area with original voids including Areas 1, 2 and 3, interpolation methods generate a large number of pixels with significant negative differences and 'overestimate' the slope in the ridge and valley regions. Moreover, in the areas with artificial voids, the diagonal lines with high slope differences can be observed in the results of interpolation methods. In addition, the results of CGAN and TKCGAN also present large slope differences around a part of valleys especially in the areas with artificial voids. However, their spatial distribution patterns in the areas with original voids are not as clear as those of interpolation methods, and the results indicate most errors exist in the two sides of ridges and

valleys.

Furthermore, we analyse the relationship between slope MAE and slope and illustrate it in Figure 9. The results of interpolation methods still maintain an increasing trend with the increase of slope, while the results of TKCGAN show a significant trend of initial decrease and following increase. These phenomena are consistent with what we observed in Section 3.1. Generally, in the areas with gentle slope, interpolation methods achieve low elevation and slope differences. However, with the increase of slope, TKCGAN outperforms other methods especially in the regions with medium slopes. Besides, TKCGAN has similar trends with CGAN which indicate that this special trend might be resulted by the traditional GAN configuration.

Therefore, it can be concluded that on the one hand, compared with the interpolation methods, our method can achieve low errors and differences in areas with medium and high slopes; on the other hand, TKCGAN efficiently reduces the error in regions with low and high slopes compared with CGAN. These phenomena both exist in Rocky Mountain and Himalayas Mountain regions. Therefore, we suggested to applied this method in areas with high terrain relief, while in the flat areas, the interpolation methods lead to low error.

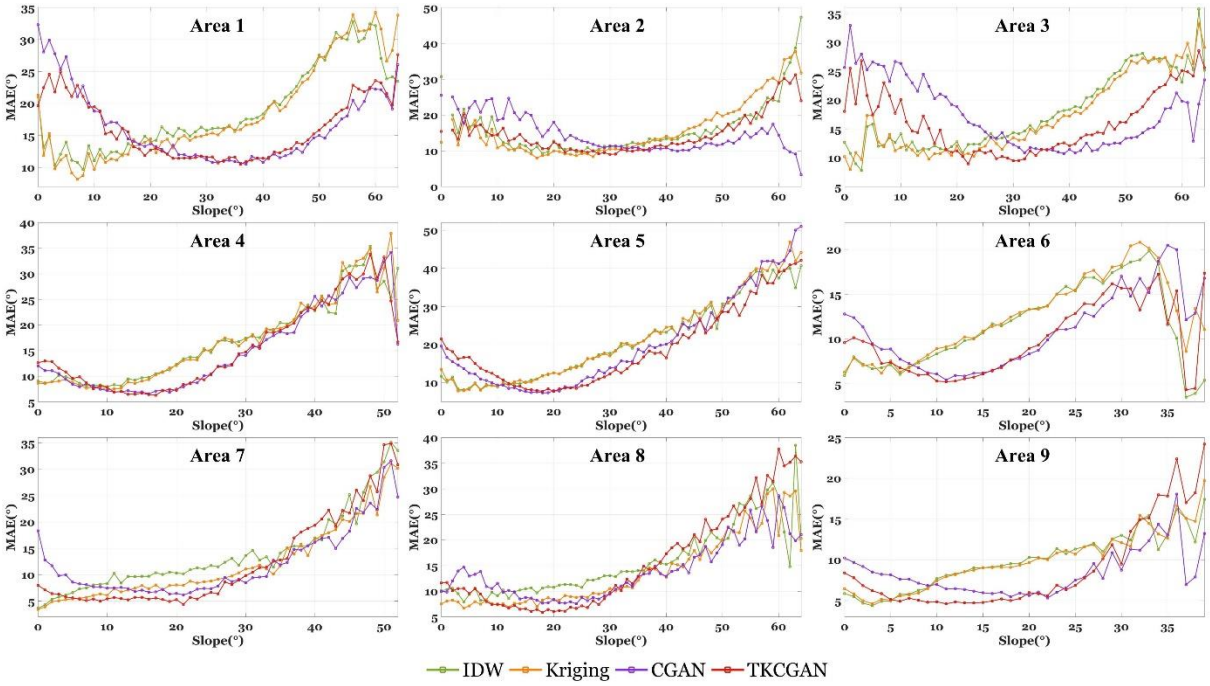


**Figure 9.** The statistical relationship between slope MAE and surface slope of different areas.

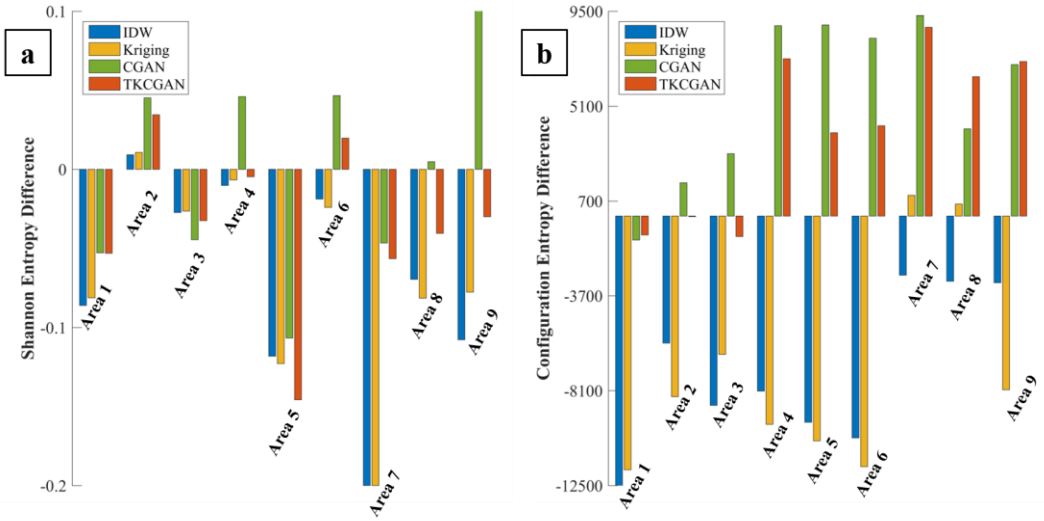


**Figure 10**. Shannon entropy and configuration entropy differences of the compared methods in the test areas

Moreover, the comparison of entropy difference shown in Figure 10 also support that TKCGAN generally outperforms other methods in the terrain reconstruction. The IDW and kriging interpolation methods tend towards low entropy differences in areas with small voids, including Areas 7, 8 and 9, while significant information loss occur in other areas with original

voids and large manually produced voids. Besides, generally, SE reflects that the CGAN results in more loss of information than the TKCGAN, while the CE entropy differences further indicate that the TKCGAN reconstructs terrain with a more similar spatial configuration to that the reference data than the CGAN. It must be noted that almost all CGAN's difference are positive. This indicates that a part of terrain information not expressed by the reference data is generated by the CGAN because of its inferential capability.

### 3.4 Reconstruction of key terrain features

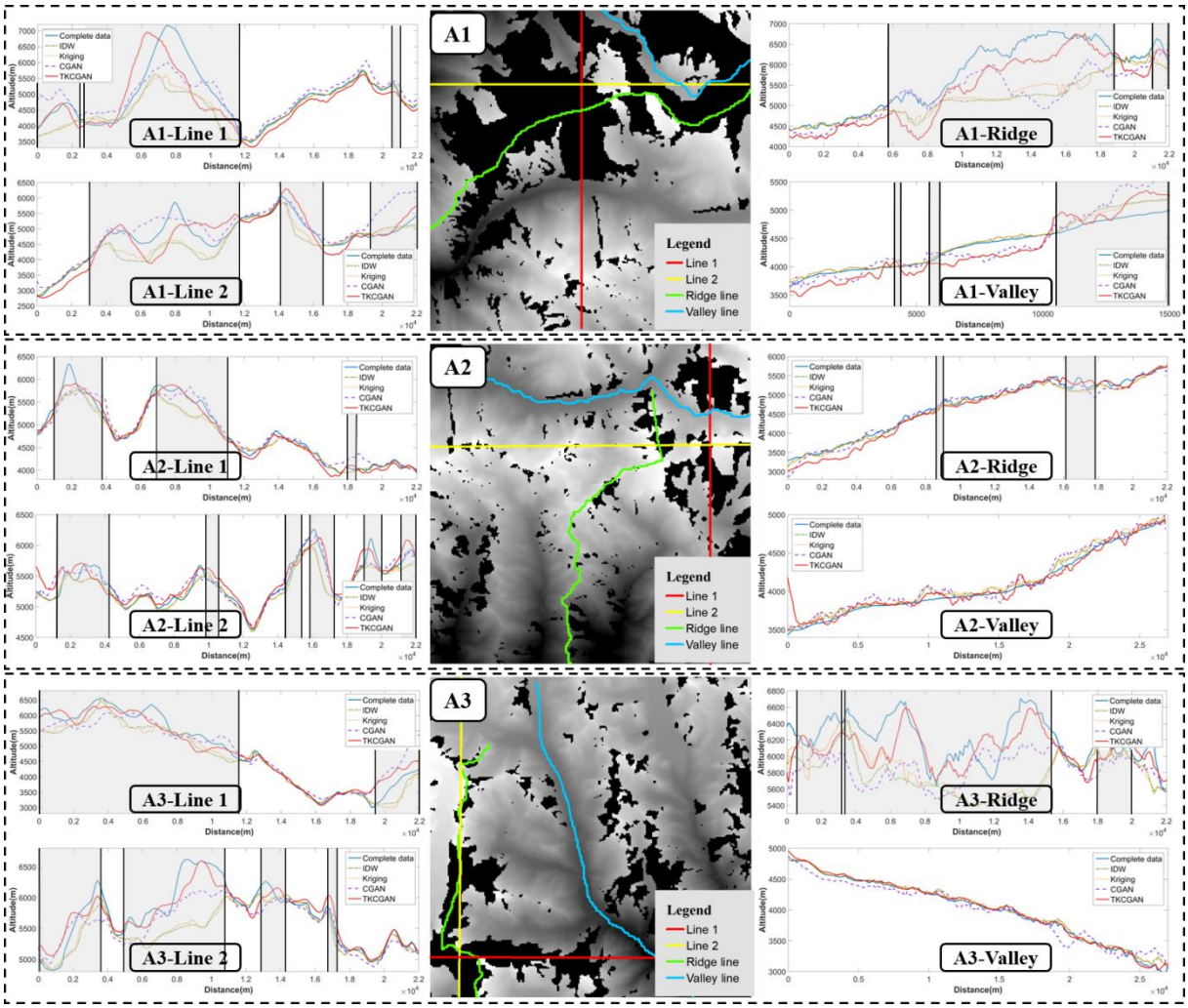


**Figure 11**. Cross sections in different study areas. (A1, A2 and A3 in this figure represent same areas of Area 1, Area 2 and Area 3 in Figure 5, respectively. Line 1 and Line 2 in

different areas are manually selected lines; ridge lines and valley lines are natural terrain feature lines; grey boxes represent void areas.)

**Table 4.** Elevation accuracy of voids on the selected profiles

(The valley lines in Area 2 and Area 3 has no overlap with voids)

| | MAE of Line 1 (m) | | | | MAE of Line 2 (m) | | | |
|---|---|---|---|---|---|---|---|---|
| | IDW | Kriging | CGAN | TKCGAN | IDW | Kriging | CGAN | TKCGAN |
| **Area 1** | 342.34 | 319.75 | **190.04** | 247.02 | 271.73 | 232.05 | **191.26** | 193.22 |
| **Area 2** | 68.32 | 66.19 | 47.35 | **24.93** | 32.82 | 35.49 | 21.48 | **21.21** |
| **Area 3** | 221.62 | 203.37 | 248.62 | **149.23** | 186.54 | 177.92 | 113.43 | **67.47** |

| | MAE of Ridge (m) | | | | MAE of Valley (m) | | | |
|---|---|---|---|---|---|---|---|---|
| | IDW | Kriging | CGAN | TKCGAN | IDW | Kriging | CGAN | TKCGAN |
| **Area 1** | 557.18 | 527.13 | 345.37 | **317.96** | 57.71 | **51.33** | 122.57 | 67.54 |
| **Area 2** | 22.59 | 25.07 | **11.25** | 16.62 | – | – | – | – |
| **Area 3** | 328.10 | 284.20 | 256.16 | **137.97** | – | – | – | – |

Three study areas with original data voids are used to analyse the performances of different methods from the perspective of profile maps. The IDW and kriging interpolation methods generate reliable terrain in relatively flat areas, such as the valleys and ridges in A2 (as shown in Figure 11 A2-Ridge and A2-Valley). However, the unfavourable results generated by the interpolation methods can be observed in areas with intense terrain relief (Figure 11 A1-Line1 and A3-Ridge), and this phenomenon can also be presented by the comparison of quantitative metrics in Table 4. Moreover, in Figure 11 A1-Line2, A2-Line1 and A3-Line1, CGAN and TKCGAN successfully reconstruct terrain that basically matches the profiles of real surface depicted by the complete data. The quantitative metrics further indicates that TKCGAN achieves lower elevation differences compared with other methods.

However, some unexpected results can still be observed in the TKCGAN outputs. For example, the possibility of redundant relief exists in some flat areas (Figure 11 A1-Valley and

A2-Valley), and valley regions are pulled down to inaccurate altitudes (Figure 11 A1-Ridge). Through an analysis of the produced profile maps and the related quantitative metrics, it can be found that the terrains around valleys and ridges are almost restored by the TKCGAN as we expected. This phenomenon matches what we found before: the TKCGAN retains a large amount of terrain information, which is reflected by the corresponding low elevation, slope and entropy differences. Even we cannot generate pixel values that are same as corresponding pixels in the reference data, TKCGAN still outperforms other methods through the analysis of topographic characteristics.

## 4. Discussions

### 4.1 Use of topographic knowledge in deep learning-based algorithms

Deep learning-based algorithms have been proven to significantly improve the accuracy and efficiency of remote sensing-related studies (Li and Hsu, 2020; Janowicz et al., 2020; Qiu et al., 2019). Previous studies have discussed the integration of semantic information or perceptive knowledge into deep learning algorithms in the field of human activities and natural processes (Li and Hsu, 2020; Zhao et al., 2017), which have achieved good performances in the related applications especially in urban regions (Janowicz et al., 2020; Zhao et al., 2017). But the fundamental knowledge about natural objects contains more uncertainty and vague definition than that of human-related objectives, and it is still challengeable to concatenate these natural knowledge with deep learning models. For DEMs, which have some different characteristics compared to those of general imagery and represent the altitude of surface, more geographical knowledge should be considered when constructing of deep learning-based

algorithms for DEM-related studies (Dong et al., 2020). In this study, the good results achieved by the TKCGAN represent that the construction of loss functions is a practical way to model and integrate topographic knowledge into deep learning-based models and improve the reasonability of terrain relief. The results also show that our strategy, which combines topographic knowledge and deep learning-based algorithms, can be used in data with different spatial resolutions and voids with various sizes. In addition, a similar strategy can also be used for other landform regions and for other remote sensing data. For different landform regions, the key topographic knowledge and the corresponding constraints used in this strategy can be adopted even if the terrain characteristics change across different study areas. Besides, the proposed strategy can be viewed as an attempt to transform perceptive natural knowledge to quantitative rules in state-of-art algorithms. The similar transformation can also be used in other data such as imagery and point clouds.

However, several problems still need to be discussed in the future. A part of unexpected relief artefacts that are larger than the real surface can be found, especially in the valley areas, and this is because the proposed algorithm combining terrain-constrained loss functions tend to generate steeper terrain to obtain small loss values during the training process. In the future, the novel model with an adaptive size of analysing window could be possible to integrate more contextual information and eliminate this type of error. Additionally, a line map that does not contain enough content about terrain feature lines could have a negative influence on the restored DEM. As shown in Figure 12, because of the lack of information about ridges (marked by blue circles), the TKCGAN cannot generate detailed terrain in these areas. The missing lines mostly representing the minor ridges and valleys possibility caused by the visual interpretation

based on remote sensing imagery in the process of data preparation. This disadvantage could be solved by the integration of various line map sources generating by different ways, including automated extraction from imagery or interpretation based on the topographic maps.

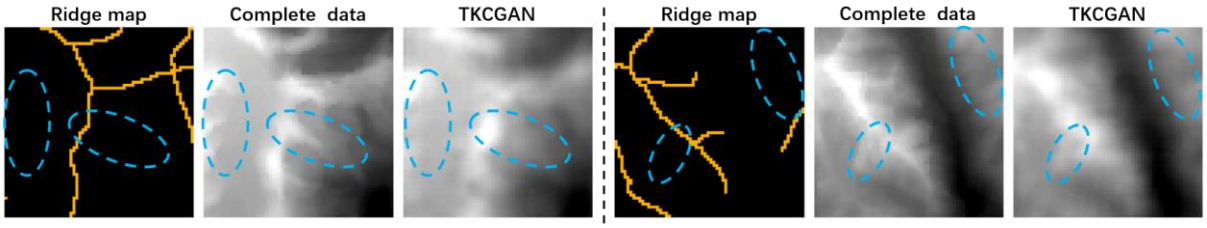


**Figure 12**. Inaccurate reconstruction because of the lack of corresponding ridge lines

### 4.2 Effect of terrain information on remote sensing-based algorithms

The terrain effect is an important factor that needs to be considered in remote sensing studies focusing on the calculation of environmental indices and factors (He et al., 2019). Some common remote sensing indices, such as solar radiation, land surface temperature and leaf area indices, are significantly influenced by the topographic characteristics (He et al., 2019; Jin et al., 2017; Zhao et al., 2019). On the one hand, the complexity and heterogeneity of land surfaces, especially rugged surfaces, result in strong topographic variations and intense changes in topographic characteristics (Wu et al., 2019; Yan et al., 2020). This leads to an intense disturbance of the signals received by the sensors and reduces the usability of retrieval algorithms designed for flat areas. On the other hand, complex surface shapes, especially in mountainous areas, induce complex characteristics in the patterns of ecological, hydrological, and meteorological parameters (He et al., 2019). These complex parameters compose a fragile and sensitive ecosystem in areas with large elevation gradients and increase the uncertainty of retrieval algorithms. DEM data that accurately express topographic characteristics can provide

various and precise terrain factors, which can be integrated into traditional retrieval algorithms to reduce the terrain effect and correct the produced retrieval results. The strategy we propose here can support the construction of a sophisticated relationship model between a retrieval algorithm and terrain and improve the calculation of appropriate retrieval results for various environmental indices.

## 5. Conclusions

In this research, we attempted to integrate fundamental topographic knowledge into the process of DEM reconstruction and construct a deep learning-based model called the TKCGAN. The TKCGAN uses terrain feature lines as additional input data and learns topographic characteristics based on these input features. Topographic knowledge around valleys and ridges is reframed to form novel loss functions that guide neural networks to fill DEM voids with reliable terrain. The TKCGAN integrated with these new loss functions effectively addresses the unsatisfactory reconstruction of DEM voids that violate topographic knowledge-based cues. A comparison between the TKCGAN and other methods shows that the TKCGAN outperforms traditional interpolation methods and the traditional CGAN especially in the slope expression. The integration strategy used in the TKCGAN increases the elevation and slope accuracy of the network at the pixel level and improves the quality of the restored DEM. Additionally, on the one hand, the input terrain features and topographical knowledge are replaceable, which means that the proposed strategy can be used to reconstruct void-filled DEMs across different environments with various topographic characteristics. On the other hand, the proposed strategy can also fill DEM voids with different spatial resolutions and voids with various sizes. These

two advantages significantly widen the applicability of this strategy. In the future, it could be possible to extend the TKCGAN model to other data refinement tasks, such as those involving remote sensing imagery and light detection and ranging (LiDAR) data. In addition, related studies that need to integrate topographic characteristics or reduce the terrain effect can benefit from DEMs reconstructed by our method. Especially in areas with rugged surfaces, the TKCGAN is able to reconstruct reliable terrain in void areas and provide more DEMs that can support the analyses of environmental factors and geographic processes.

## Declaration of Competing Interest

The authors declare that they have no known competing financial interests or personal relationships that could have appeared to influence the work reported in this paper.

## Acknowledgments

This work was supported by National Natural Science Foundation of China [grant number: No. 41930102, No. 41971333]; and Priority Academic Program Development of Jiangsu Higher Education Institutions.

## Reference

[dataset] Shuttle Radar Topography Mission (SRTM) Non-Void Filled. USGS. https://doi.org/10.5066/F7K072R7

[dataset] Shuttle Radar Topography Mission (SRTM) Void Filled. USGS.

https://doi.org/10.5066/F7F76B1X

Arun, P., 2013. A comparative analysis of different DEM interpolation methods. The Egyptian Journal of Remote Sensing and Space Science, 16, 133-139. https://doi.org/10.1016/j.ejrs.2013.09.001

Boulton, S., Stokes, M., 2018. Which DEM is best for analyzing fluvial landscape development in mountainous terrains? Geomorphology, 310, 168-187. https://doi.org/10.1016/j.geomorph.2018.03.002

Callow, J., Van Niel, K., Boggs, G., 2007. How does modifying a DEM to reflect known hydrology affect subsequent terrain analysis?. Journal of hydrology, 332(1-2), 30-39.

Cheng, X., Li, Z., 2021a Configurational Entropy for Optimizing the Encryption of Digital Elevation Model Based on Chaos System and Linear Prediction. Applied Sciences, 11, 2402. https://doi.org/10.3390/app11052402

Cheng, X., Li, Z., 2021b. Using Boltzmann Entropy to Measure Scrambling Degree of Grayscale Images. In 2021 IEEE 5th International Conference on Cryptography, Security and Privacy (CSP), 181-185. IEEE. https://doi.org/10.1109/CSP51677.2021.9357492

Chou, T.Y., M.L. Yeh, Y.C. Chen, and Y.H. Chen, 2010. Disaster monitoring and management by the unmanned aerial vehicle technology, Proceedings of the ISPRS TC VII Symposium (W. Wagner and B. Székely, editors), Vienna, Austria, Vol. XXXVIII, Part 7B, pp. 137–142.

Dong, G., Chen, F., Ren, P., 2018. Filling SRTM void data via conditional adversarial networks. In IGARSS 2018-2018 IEEE International Geoscience and Remote Sensing Symposium, 7441-7443. IEEE. https://doi.org/10.1109/IGARSS.2018.8518992

Dong, G., Huang, W, Smith, W, Ren, P., 2019 Filling Voids in Elevation Models Using a Shadow-Constrained Convolutional Neural Network. IEEE Geoscience and Remote Sensing Letters, 17, 592-596. https://doi.org/10.1109/LGRS.2019.2926530

Dong, G., Huang, W, Smith, W, Ren, P., 2020. A shadow constrained conditional generative adversarial net for SRTM data restoration. Remote Sensing of Environment, 237, 111602. https://doi.org/10.1016/j.rse.2019.111602

Evans, I., 2012. Geomorphometry and landform mapping: What is a landform?. Geomorphology, 137(1), 94-106. https://doi.org/10.1016/j.geomorph.2010.09.029

Farr, T., Rosen, P., Caro, E., Crippen, R., Duren, R., Hensley, S., Kobrick, M., Paller, M., Rodriguez, E., Roth, L. and Seal, D., 2007. The shuttle radar topography mission. Reviews of geophysics, 45(2). https://doi.org/10.1029/2005RG000183

Gao, P., Zhang, H., Li, Z., 2017. A hierarchy-based solution to calculate the configurational entropy of landscape gradients. Landscape ecology, 32, 1133-1146. https://doi.org/10.1007/s10980-017-0515-x

Geman, S., Geman, D., 1984. Stochastic relaxation, Gibbs distributions, and the Bayesian restoration of images. IEEE Transactions on pattern analysis and machine intelligence, 721-741. https://doi.org/10.1109/TPAMI.1984.4767596

Goodfellow, I., Pouget-Abadie, J., Mirza, M., Xu, B., Warde-Farley, D., Ozair, S., Courville, A., Bengio Y., 2014. Generative adversarial nets. In: Advances in Neural Information Processing Systems (NIPS).

Grohman, G., Kroenung, G., Strebeck, J., 2006. Filling SRTM voids: The delta surface fill method. Photogrammetric Engineering and Remote Sensing, 72, 213-216.

689 Guilbert, E., Moulin, B., 2017. Towards a common framework for the identification of
690 landforms on terrain models. ISPRS international journal of geo-information, 6, 12.
691 https://doi.org/10.3390/ijgi6010012
692 Hall, O., Falorni, G., Bras, R., 2005 Characterization and quantification of data voids in the
693 shuttle radar topography mission data. IEEE Geoscience and Remote Sensing Letters, 2,
694 177-181. https://doi.org/10.1109/LGRS.2004.842447
695 He, J., Zhao, W., Li, A., Wen, F., Yu, D., 2019. The impact of the terrain effect on land surface
696 temperature variation based on Landsat-8 observations in mountainous areas. International
697 Journal of Remote Sensing, 40, 1808-1827.
698 https://doi.org/10.1080/01431161.2018.1466082
699 Heritage, G., Milan, D., Large, A., Fuller, I., 2009. Influence of survey strategy and
700 interpolation model on DEM quality. Geomorphology, 112, 334-344.
701 https://doi.org/10.1016/j.geomorph.2009.06.024
702 Hirt, C., 2018. Artefact detection in global digital elevation models (DEMs): The Maximum
703 Slope Approach and its application for complete screening of the SRTM v4. 1 and MERIT
704 DEMs. Remote Sensing of Environment, 207, 27-41.
705 https://doi.org/10.1016/j.rse.2017.12.037
706 Janowicz, K., Gao, S., McKenzie, G., Hu, Y., Bhaduri, B., 2020. GeoAI: Spatially explicit
707 artificial intelligence techniques for geographic knowledge discovery and beyond.
708 International Journal of Geographical Information Science, 34(4), 625–636.
709 https://doi.org/10.1080/13658816.2019.1684500
710 Jin, H., Li, A., Bian, J., Nan, X., Zhao, W., Zhang, Z., Yin, G., 2017. Intercomparison and

711 validation of MODIS and GLASS leaf area index (LAI) products over mountain areas: A
712 case study in southwestern China. International Journal of Applied Earth Observation and
713 Geoinformation, 55, 52-67. https://doi.org/10.1016/j.jag.2016.10.008
714 Jing, C., Shortridge, A., Lin, S., Wu, J., 2014. Comparison and validation of SRTM and ASTER
715 GDEM for a subtropical landscape in Southeastern China. International Journal of Digital
716 Earth, 7, 969-992. https://doi.org/10.1080/17538947.2013.807307
717 Karkee, M., Steward, B., Abd Aziz, S., 2008. Improving quality of public domain digital
718 elevation models through data fusion. Biosystems Engineering, 101, 293-305.
719 https://doi.org/10.1016/j.biosystemseng.2008.09.010
720 LeCun, Y., Bengio, Y., Hinton, G., 2015. Deep learning. nature 521 (7553), 436-444.
721 https://doi.org/10.1038/nature14539
722 Li, S., Xiong, L., Hu, G., Dang, W., Tang, G., Strobl., J 2020a, Extracting check dam areas from
723 high-resolution imagery based on the integration of object-based image analysis and deep
724 learning. Land Degradation & Development. https://doi.org/10.1002/ldr.3908
725 Li, S., Xiong, L., Tang, G., Strobl, J., 2020b Deep learning-based approach for landform
726 classification from integrated data sources of digital elevation model and imagery.
727 Geomorphology, 354, 107045. https://doi.org/10.1016/j.geomorph.2020.107045
728 Li, W., Hsu, C., 2020. Automated terrain feature identification from remote sensing imagery: a
729 deep learning approach. International Journal of Geographical Information Science, 34,
730 637-660. https://doi.org/10.1080/13658816.2018.1542697
731 Li, W., Zhou, B., Hsu, C., Li, Y., Ren, F., 2017. Recognizing terrain features on terrestrial
732 surface using a deep learning model: An example with crater detection. In Proceedings of

the 1st Workshop on Artificial Intelligence and Deep Learning for Geographic Knowledge Discovery, 33-36. https://doi.org/10.1145/3149808.3149814

Ling, F., Zhang, Q., Wang, C., 2007. Filling voids of SRTM with Landsat sensor imagery in rugged terrain. International Journal of Remote Sensing, 28, 465-471. https://doi.org/10.1080/01431160601075509

Lu, H., Fu, X., Liu, C., Li, L., He, Y., Li, N., 2017. Cultivated land information extraction in UAV imagery based on deep convolutional neural network and transfer learning. Journal of Mountain Science, 14, 731-741. https://doi.org/10.1007/s11629-016-3950-2

Milan, D., Heritage, G., Large, A., Fuller, I., 2011. Filtering spatial error from DEMs: Implications for morphological change estimation. Geomorphology, 125, 160-171. https://doi.org/10.1016/j.geomorph.2010.09.012

Mirza, M., Osindero, S. 2014. Conditional generative adversarial nets. arXiv:1411.1784.

Ozouville, N., Deffontaines, B., Benveniste, J., Wegmüller, U., Violette, S., de Marsily, G., 2008. DEM generation using ASAR (ENVISAT) for addressing the lack of freshwater ecosystems management, Santa Cruz Island, Galapagos. Remote Sensing of Environment, 112, 4131-4147. https://doi.org/10.1016/j.rse.2008.02.017

Qiu, Z., Yue, L., Liu, X., 2019. Void Filling of Digital Elevation Models with a Terrain Texture Learning Model Based on Generative Adversarial Networks. Remote Sensing, 11, 2829. https://doi.org/10.3390/rs11232829

Reuter, H., Nelson, A. Jarvis, A., 2007. An evaluation of void-filling interpolation methods for SRTM data. International Journal of Geographical Information Science, 21, 983-1008. https://doi.org/10.1080/13658810601169899

Robinson, N., Regetz, J., Guralnick, R., 2014. EarthEnv-DEM90: A nearly-global, void-free, multi-scale smoothed, 90m digital elevation model from fused ASTER and SRTM data. ISPRS Journal of Photogrammetry and Remote Sensing, 87, 57-67. https://doi.org/10.1016/j.isprsjprs.2013.11.002

Sesnie, S., Gessler, P., Finegan, B., Thessler, S., 2008. Integrating Landsat TM and SRTM-DEM derived variables with decision trees for habitat classification and change detection in complex neotropical environments. Remote Sensing of Environment, 112, 2145-2159. https://doi.org/10.1016/j.rse.2007.08.025

Shannon, C., 1948. A mathematical theory of communication. The Bell system technical journal, 27(3), 379-423. https://doi.org/10.1002/j.1538-7305.1948.tb01338.x

Shuttle Radar Topography Mission, 2021. Jet Propulsion Laboratory. https://www2.jpl.nasa.gov/srtm/

Wang, G., Gertner, G., Parysow, P., Anderson, A., 2001. Spatial prediction and uncertainty assessment of topographic factor for revised universal soil loss equation using digital elevation models. ISPRS Journal of Photogrammetry and Remote Sensing, 56, 65-80. https://doi.org/10.1016/S0924-2716(01)00035-1

Wei, H., Xiong, L., Tang, G., Strobl, J., Xue, K., 2021. Spatial–temporal variation of land use and land cover change in the glacial affected area of the Tianshan Mountains. Catena, 202, 105256. https://doi.org/10.1016/j.catena.2021.105256

Wu, S., Wen, J., Gastellu-Etchegorry, J., Liu, Q., You, D., Xiao, Q., Hao, D., Lin, X., Yin, T., 2019. The definition of remotely sensed reflectance quantities suitable for rugged terrain. Remote Sensing of Environment, 225, 403-415. https://doi.org/10.1016/j.rse.2019.01.005

Xiong, L., Tang, G., Li, F., Yuan, B., Lu, Z., 2014. Modeling the evolution of loess-covered landforms in the Loess Plateau of China using a DEM of underground bedrock surface. Geomorphology, 209, 18-26. https://doi.org/10.1016/j.geomorph.2013.12.009

Xiong, L., Tang, G., Yang, X., Li, F., 2021. Geomorphology-oriented digital terrain analysis: Progress and perspectives. Journal of Geographical Sciences, 31, 456-476. https://doi.org/10.1007/s11442-021-1853-9

Yan, G., Jiao, Z., Wang, T., Mu, X., 2020. Modeling surface longwave radiation over high-relief terrain. Remote Sensing of Environment, 237, 111556. https://doi.org/10.1016/j.rse.2019.111556

Yuan, Q., Shen, H., Li, T., Li, Z., Li, S., Jiang, Y., Xu, H., Tan, W., Yang, Q., Wang, J. and Gao, J., 2020. Deep learning in environmental remote sensing: Achievements and challenges. Remote Sensing of Environment, 241, p.111716.

Zhao, W., Duan, S., Li, A., Yin, G., 2019. A practical method for reducing terrain effect on land surface temperature using random forest regression. Remote Sensing of Environment, 221, 635-649. https://doi.org/10.1016/j.rse.2018.12.008

Zhao, W., Du, S., Wang, Q., Emery, W., 2017. Contextually guided very-high-resolution imagery classification with semantic segments. ISPRS journal of photogrammetry and remote sensing, 132, 48-60. https://doi.org/10.1016/j.isprsjprs.2017.08.011

Zheng, X., Xiong, H., Yue, L. and Gong, J., 2016. An improved ANUDEM method combining topographic correction and DEM interpolation. Geocarto International, 31(5), 492-505. https://doi.org/10.1080/10106049.2015.1059899

Zhu, D., Cheng, X., Zhang, F., Yao, X., Gao, Y., Liu, Y., 2020. Spatial interpolation using

conditional generative adversarial neural networks. International Journal of Geographical Information Science, 34, 735-758. https://doi.org/10.1080/13658816.2019.1599122